Appl Phys B (2010) 99: 149–157
DOI 10.1007/s00340-009-3835-y

Applied Physics B
Lasers and Optics

1-mJ, sub-5-fs carrier–envelope phase-locked pulses

X. Chen · L. Canova · A. Malvache · A. Jullien · R. Lopez-Martens · C. Durfee · D. Papadopoulos · F. Druon

Received: 20 September 2009 / Revised version: 6 November 2009 / Published online: 1 December 2009

Abstract We report the routine generation of sub-5-fs laser pulses with 1-mJ energy and stable carrier–envelope phase at 1-kHz repetition rate, obtained by compressing the multi-mJ output from a phase-locked Ti:sapphire amplifier in a rare-gas-filled hollow fiber. The dual-stage amplifier features a hybrid transmission grating/chirped mirror compressor providing 2.2-mJ, 26-fs pulses at 1 kHz with standard phase deviation of 190 mrad rms. We demonstrate hour-long phase stability without feedback control of grating position or rigorous control of the laser environment, simply by using small pulse stretching factors in the amplifier, which minimize the beam pathway in the compressor. The amplifier also integrates a versatile AOPDF (acousto-optic programmable dispersive filter) for closed-loop spectral phase optimization. The various factors influencing the overall phase stability of the system are discussed in detail. Using the optimized output, 1-mJ, 4.5-fs pulses are generated by seeding the neon gas filled hollow fiber with a circularly polarized input beam. A standard phase deviation of 230 mrad after the HCF is obtained by direct f-to-2f detection and slow-loop feedback to the oscillator locking electronics without any additional spectral broadening.

X. Chen (✉) · L. Canova · A. Malvache · A. Jullien · R. Lopez-Martens
Laboratoire d'Optique Appliquée, ENSTA ParisTech, CNRS, Ecole Polytechnique, 91761 Palaiseau Cedex, France
e-mail: xiaowei.chen@ensta.fr

X. Chen
State Key Laboratory of High Field Laser Physics, Shanghai Institute of Optics and Fine Mechanics, Chinese Academy of Sciences, Shanghai 201800, China

C. Durfee
Department of Physics, Colorado School of Mines, 1523 Illinois St., Golden, CO 80401, USA

D. Papadopoulos · F. Druon
UMS 3502, Institut de la Lumiére Extrême, 91761 Palaiseau Cedex, France

D. Papadopoulos · F. Druon
Laboratoire Charles Fabry de l'Institut d'Optique, CNRS, Université Paris-Sud, 91127 Palaiseau, France

1 Introduction

Stabilizing the carrier–envelope phase (CEP) of ultra-short laser pulses has provided tremendous thrust to strong-field physics in recent years [1, 2], especially in the case of few-cycle pulses where the pulse intensity varies almost as quickly as the laser electric field itself. In particular, CEP-controlled few-cycle pulses with sub-mJ energy in the near-infrared region have been used to demonstrate isolated attosecond pulse generation in the extreme ultraviolet via high-harmonic generation in gases [3–5]. Today, CEP-locked few-cycle pulses of several mJ are needed to increase both the brightness and the spectral range of current attosecond light sources. Moreover, it has been suggested that such pulses could open the way to exploring relativistic intensity laser–matter interactions at kHz repetition rate [6].

However, pulses from a conventional femtosecond Ti:sapphire (Ti:Sa) chirped pulse amplifier (CPA) are usually limited in duration by gain narrowing to around 20 fs [7, 8] and one must rely on nonlinear post-compression schemes, such as hollow-core-fiber (HCF) compressors [9], optical filaments [10] or the newly developed planar hollow waveguide technique [11], in order to reach the few-cycle regime. Achieving this at the multi-mJ level while preserving the CEP of the pulses therefore requires a multi-mJ, sub-30-fs front-end CPA laser system with reliable long-term

CEP stability as well as a post-compression device that can be scaled in energy to handle the higher input flux without deteriorating the initial CEP stability.

2 CEP stabilization

The first aspect we must deal with is CEP stabilization inside the CPA laser chain. This is usually done first by stabilizing the CEP offset of the oscillator [12, 13] and by subsequently pre-compensating the slow drift introduced during amplification, typically at 1-kHz repetition rate [14]. This slow drift originates chiefly from mechanical vibrations and air fluctuations in open space dispersive elements, such as the stretcher and compressor [15–17]. Historically, the first CPA system to achieve CEP stabilization featured a bulk material stretcher followed by a prism compressor and typically delivered sub-mJ energies [14]. To achieve higher energies, however, longer pulse, grating-based CPA systems remain particularly attractive. CEP stabilization has recently been demonstrated with this type of system by controlling the grating position in either the stretcher [18] or the compressor [19, 20] in order to improve the shot-to-shot CEP fluctuations of the amplified pulses.

We recently reported a 2.2-mJ, 26-fs system at 1 kHz featuring excellent CEP stability over extended periods of time [21]. This CPA system relies on moderate pulse chirping through bulk material, which permits the use of transmission gratings with a very compact footprint. In our case, the reduced pulse duration leads to high propagation intensities inside the amplifier and hence to the accumulation of a relatively high B-integral. This can singularly deteriorate the spatial and temporal quality of the output pulses. Since self-phase modulation in the amplifier's materials is the main source of the B-integral, the spectral phase of the amplified pulses now becomes a function of the pulse energy, calling for careful management of the nonlinear (as well as linear) phase throughout the system using adaptive phase compensation techniques [22].

3 HCF compression at high energies

The second aspect we must deal with is the post-compression of multi-mJ pulses with preservation of the initial CEP. HCF compressors are widely used to deliver few-cycle pulses for attosecond science [1–5]. Confinement of the laser beam inside the waveguide ensures spatially uniform broadening as well as an excellent output beam profile [23]. HCF compressors with static gas pressures have been successfully made to achieve two-cycle pulses with energies on the order of 1 mJ [24, 25]. Beyond this, the achievable output energy is promptly limited by the interplay of self-focusing and ionization, which couples energy into higher-order propagation modes of the waveguide and results in significant losses and instability. One way to go around this problem is to apply a pressure gradient across the HCF, which helps delay these effects and keep more pulse energy in the fundamental mode of the fiber [26]. This approach has enabled the generation of two-cycle pulses with several mJ of energy [27, 28] and, just recently, of 1.5-cycle pulses beyond 1 mJ [29].

An alternative approach for increasing the energy throughput of a statically filled HCF is to seed the fiber with circularly polarized pulses [30, 31]. Compared to the case of linear polarization at the same given intensity, circular polarization has the benefit of diminishing the Kerr effect [32], while increasing the ionization threshold [33]. This means that higher-energy pulses can be propagated through the fiber using a circularly polarized input beam. This approach also offers a significant improvement of the long-term spectral stability of the output pulses, which has a direct influence on the preservation of the CEP after the fiber. Until now, the benefits of circular polarization have mainly been demonstrated in filamentation experiments [34–38] but much less explored in the case of HCF compressors.

4 Experimental progress at LOA

In this communication, we describe a Ti:Sa CPA system delivering CEP-stable, 2.2-mJ, 26-fs pulses at 1 kHz, which features a bulk material stretcher, two amplification stages and a compact hybrid compressor composed of transmission gratings and chirped mirrors [21]. No active control of the grating position in the compressor is necessary for CEP stabilization. The system routinely exhibits long-term CEP stability with a 190 mrad rms phase error measured over several hours. We show that the acousto-optic programmable dispersive filter (AOPDF, Dazzler™, Fastlite) inside the amplifier chain can be used to optimize pulse compression in a closed-loop fashion [22]. The influence of the amplifier configuration on the measured output CEP fluctuations is also analyzed in detail. Finally, we demonstrate that by seeding a statically neon-filled fiber with circularly polarized pulses from the amplifier, we can routinely generate 1-mJ, 4.5-fs pulses with CEP stability comparable to that of the laser (∼230 mrad rms).

5 CEP-stabilized multi-mJ, sub-30-fs CPA laser system

Our laser system (Fig. 1) consists of a commercial 1-kHz CEP-stabilized Ti:Sa amplifier (Femtopower Compact Pro CE Phase, Femtolasers GmbH) followed by a home-built Ti:Sa multi-pass amplifier. The two amplification stages are respectively pumped by 11 and 20 W from a single 1-kHz

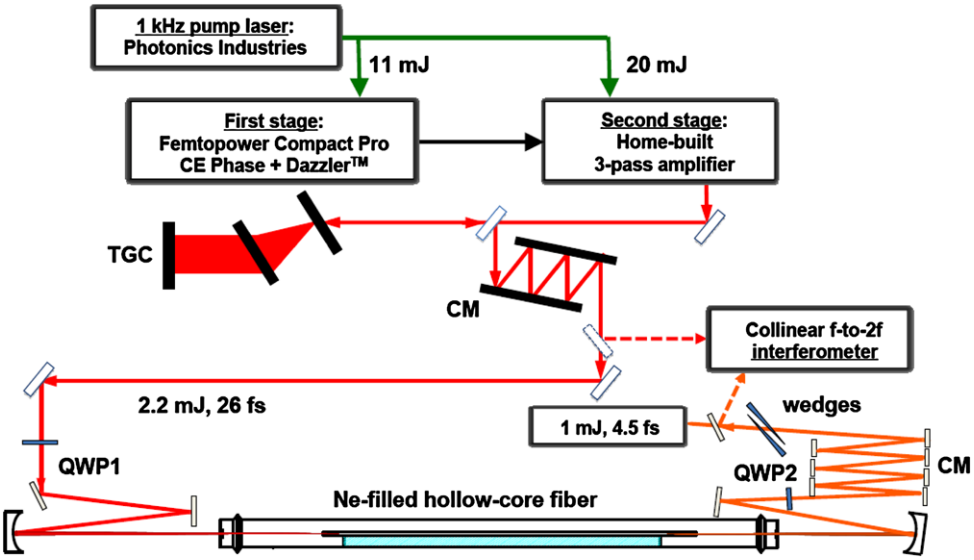

Fig. 1 Schematic of the CEP-stable, mJ-level, sub-5-fs laser system, including a CEP-stable, 2.2-mJ, 26-fs, 1-kHz CPA laser system with transmission grating (TGC)/chirped mirror (CM) hybrid compressor, and a hollow-fiber compressor. QWP: broadband achromatic quarter-wave plate

frequency-doubled Q-switched Nd:YLF laser (DM 50 series, Photonics Industries). The onboard Ti:Sa oscillator (Rainbow, Femtolasers GmbH) is CEP locked with a typical rms error better than 50 mrad [39]. The pulses from the oscillator are first over-stretched through a 20-cm SF57 glass block unit and sent into the first four passes of the amplifier to reach the μJ level. The amplified pulse train then passes through the AOPDF (low-jitter Dazzler HR-45-800, Fastlite) with roughly 40% efficiency over 120-nm bandwidth. Situated between passes four and five of the amplifier, the AOPDF can efficiently fight gain narrowing in the rest of the system and be used to measure and optimize the spectral phase of the output pulses downstream. After this, the pulses are sent through a Pockels cell (Bergmann Messgeräte Entwicklung KG, BME) to select a 1-kHz train of CEP-locked pulses to be amplified in the next six passes up to a maximum energy of 2 mJ. Typical amplified spectral bandwidths at this point are above 50 nm, and we estimate that at this stage the pulses are stretched to about 7-ps duration.

The Femtopower output is then boosted up to the multi-mJ level in a home-made, image-relayed three-pass amplifier offering the flexibility of controlling the seed beam size on the crystal for each pass. The 8-mm-long Ti:Sa crystal (74% absorption), cut at Brewster angle, is cooled to 195 K under vacuum by a cryogenic pump (Thermo Electron GmbH). With both seed and pump beam diameters at ∼1 mm (at $1/e^2$ intensity), 750-μJ seed pulses are typically amplified to 1.7, 3.2 and 4.3 mJ respectively after each consecutive pass. For seed energies much beyond this value, modulations appear in the amplified spectrum, a signature of a high B-integral due to the small stretching factor. Consequently, the second amplifier stage is routinely seeded by 750 μJ. Gain saturation is reached in the last pass with an estimated B-integral value of ∼3 rad for the whole system.

Pulse compression is achieved using a hybrid compressor combining transmission gratings (TGC) and a highly dispersive chirped mirror pair (CM). Here, the amplified pulses are first compressed in the TGC down to ∼0.8 ps so that the peak intensity is low enough in the grating material to avoid nonlinear effects. The beam diameter is 15 mm. The TGC is composed of a pair of 600 lines/mm fused silica holographic gratings (Wasatch Photonics) separated by about 70 mm for a beam incident angle of 13.9°. The spectral phase introduced by the grating compressor is $\varphi^{(2)}_{\mathrm{TGC}} \sim -50{,}000\ \mathrm{fs}^2$ and $\varphi^{(3)}_{\mathrm{TGC}} \sim 70{,}000\ \mathrm{fs}^3$. Final compression below 30 fs is then achieved after 32 bounces on the CM ($-200\ \mathrm{fs}^2$/bounce). The residual second-order phase and positive third-order phase from the stretcher, amplifier material and compressor are compensated by the AOPDF with $\varphi^{(2)}_{\mathrm{DAZ}} = -15{,}100\ \mathrm{fs}^2$ and $\varphi^{(3)}_{\mathrm{DAZ}} = -140{,}000\ \mathrm{fs}^3$. The overall transmission efficiency of the hybrid compressor is ∼53% (∼60% for the TGC). The final compressed pulse energy is then 2.2 mJ, with an energy stability of ∼1.5% rms (∼5% for peak-to-peak), stemming mainly from the pump laser and corresponding to a standard value for kilohertz lasers.

6 Pulse optimization using the AOPDF

The AOPDF in the laser chain provides an easy and flexible way to pre-shape the seed spectrum in order to fight gain narrowing during amplification. Figure 2a shows the spectral profile of the pulse at different stages of the laser chain: after the Femtopower (uncompressed), after the second amplifier and after the hybrid compressor. There is a slight spectral narrowing observed during the amplification, but the AOPDF in the chain enables us to reproducibly produce

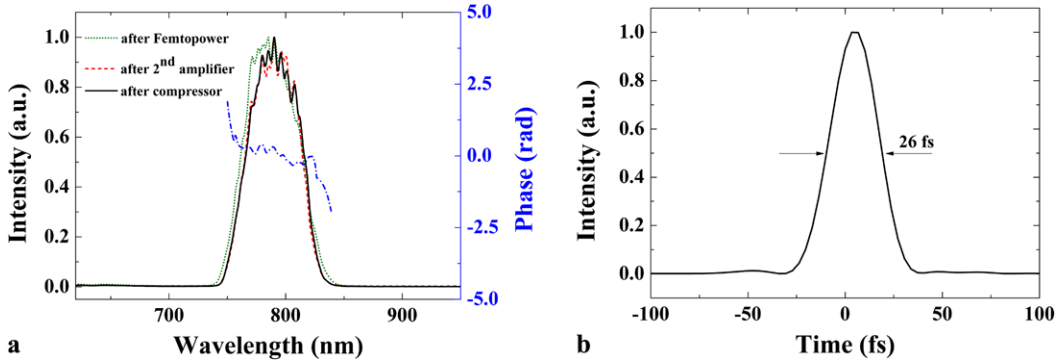

Fig. 2 (**a**) Laser spectra at different positions inside the laser system with 2.2-mJ, 26-fs laser output: after Femtopower (*dotted green line*), after the second amplifier (*dashed red line*) and after the hybrid compressor (*solid black line*), and spectral phase (*dash-dotted blue line*) of the compressed pulses measured by SPIDER; (**b**) temporal intensity profile of the compressed pulses (SPIDER)

output pulses with an excellent Gaussian spectrum of 52 nm in bandwidth (FWHM). The small ripples around the peak of the spectrum arise from the moderately high B-integral of the overall system, which does not however compromise optimal compression.

Pulse compression is optimized in a closed-loop fashion using a commercial optimization algorithm coupled to the AOPDF (DazScope^{TM}, Fastlite). Here, a small fraction of the output energy (<1 μJ) is selected by a beam splitter and focused into a 50-μm type-I BBO crystal by an $f = 500$ mm focusing lens. The generated second harmonic is filtered out and collected by a commercial spectrometer (AvaSpec-3648, Avantes). In the measurement mode, the AOPDF is set to add a sequence of pure quadratic phases (pure linear chirp) to the pulse and the second harmonic generation (SHG) spectrum is recorded for every added value of chirp [40]. Once the whole range of chirp is scanned, the second-order derivative of the input spectral phase (the 'local' chirp) is extracted based on a fit of the asymptotic decay of the SHG spectrum for large chirps. The phase is then retrieved by double integration and compensated by the Dazzler in the laser chain. The optimized output pulse duration of our laser system was measured at 26 fs with a home-built spectral phase interferometry for direct electric field reconstruction (SPIDER) device. Figure 2 shows the measured spectral phase and corresponding reconstructed temporal profile (26 fs FWHM).

7 Influence of the CPA system design on the CEP

In our laser system, the slow CEP slip of the amplified laser pulses can be measured using a commercial collinear f-to-$2f$ interferometer (APS 800, Menlo Systems) [41] and then fed back into the oscillator locking electronics. During a typical measurement, the spectrometer (Thorlabs) operates in single-shot mode (1-ms integration time) and 20 consecutive spectra are acquired within the loop-cycle time (100 ms). The CEP drift value can be obtained based on each spectrum through a FFT algorithm (FFT amplitudes below ∼20% of the average amplitude are eliminated) and then an averaged value over these 20 calculated CEP drift values is recorded and used for feedback. This slow CEP drift feedback loop typically runs at 10 Hz.

The acoustic wave driver jitter of the AOPDF inside the laser can introduce significant noise in the recorded CEP drift. For a broadband AOPDF, the typical acoustic wave delay is 23.6 μs, which corresponds to an optical delay of 3.5 ps at 800 nm. Therefore, an acoustic wave jitter, τ_{ac}, can lead to an optical jitter, τ_{opt}, of the diffracted laser beam, $\tau_{opt} = \tau_{ac} \cdot 3.5\ \text{ps}/23.6\ \mu\text{s}$, which yields a random CEP drift given by

$$\delta\varphi_{DZ} = \tau_{opt}\left(\frac{2\pi c}{\lambda}\right) = \tau_{ac}\frac{2\pi}{2.67\ \text{fs}}\frac{3.5\ \text{ps}}{23.6\ \mu\text{s}}. \quad (1)$$

This means that an acoustic wave jitter of 300 ps can introduce $\pi/30$ optical jitter. Clearly, minimizing this jitter is equivalent to minimizing the optical jitter of the laser. Therefore, in collaboration with Fastlite, we improved the acoustic wave jitter of our AOPDF from ∼300 to ∼70 ps by using a less noisy PLL (phase-locked-loop) chip in the AOPDF driver. Subsequently, the measured long-term rms CEP drift error of the first amplifier stage (using the commercial prism compressor, 0.8-mJ, 27-fs laser output, with equivalent pulse energy stability to that after the second amplifier) was dramatically reduced from ∼176 to ∼102 mrad. This shows very good agreement with the theoretical improvement value (70 mrad) calculated from (1). The improved CEP drift error value is comparable to the typical drift error (∼80 mrad rms) of the commercial Femtopower system itself without AOPDF. Figure 3a shows a long-term measurement of the stabilized CEP drift (∼102 mrad rms) of the Femtopower with an upgraded AOPDF driver. A statistical distribution of the data points over CEP drift values

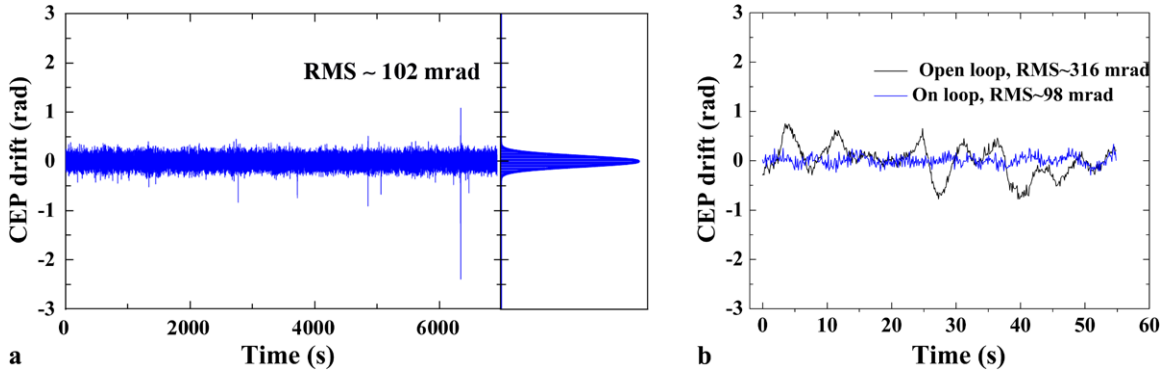

Fig. 3 CEP drift measurement of the first stage of the amplifier with 0.8-mJ, 27-fs laser output (Femtopower with commercial prism compressor). (**a**) Measured stabilized CEP drift with slow-loop control over 2 h (∼102 mrad rms), together with the statistical distribution of the data points over CEP drift values. (**b**) Comparison of CEP drift with (∼98 mrad rms, *blue line*) and without (∼316 mrad rms, *black line*) slow-loop control on a short time scale (∼1 min)

is also shown in the right-hand panel of the figure. Comparing the rms CEP drift over one minute with (∼98 mrad) and without (∼316 mrad) the slow loop (Fig. 3b), we see that the first stage of the amplifier introduces slow drifts of the CEP due to beam pointing variations and air fluctuations in the prism compressor on the few-second time scale.

The influence of the AOPDF aside, the CEP slip introduced by the amplification system originates mainly from the following three sources [15]: (1) beam pointing and temperature changes in the optical path length; (2) dispersion fluctuations in the stretcher and compressor; (3) pulse intensity fluctuations in the amplification gain medium.

Beam pointing fluctuations come from air turbulence or mechanical vibrations, which affect the shot-to-shot drift of the CEP. The CEP slip due to the variation of optical path length can be estimated by $\delta\varphi_{\mathrm{BP}} = 2\pi(\Delta L/L_{2\pi})$, where $L_{2\pi}$ is the medium length corresponding to a 2π CEP shift and ΔL is the change of optical path length. The typical $L_{2\pi}$ value at 800 nm is 157×10^3 μm for air and 37 μm for Ti:Sa crystal [15]. Generally, under good experimental conditions with beam pointing fluctuations on the order of several μrad after amplification, the CEP noise introduced is in the sub-mrad range, in other words, negligible. The influence of air and gain medium temperature variations could be more than two orders greater than that of air turbulence, but this occurs on a many-minute scale, leading only to a very slow shot-to-shot CEP drift.

The influence of beam pointing on the grating stretcher and compressor has been studied before both theoretically [17] and experimentally [18]. For a double-pass configuration, the net effects of a variation of incident angle on the CEP are small because the phase slip in the first pass can be compensated in the second pass due to the opposite incident angle change between the two passes. However, the CEP change resulting from changes in the grating separation can be on the order of 2π rad. Here we suppose that γ is the incident angle, G is the perpendicular distance between the gratings, d is the grating constant and θ is the angle between the incident and diffracted rays. Then the CEP change $\delta\varphi_{\mathrm{GD}}$ due to the separation change ΔG can be expressed by

$$\delta\varphi_{\mathrm{GD}} = 4\pi \frac{\Delta G}{d} \tan\big[\gamma - \theta(\omega_0)\big], \tag{2}$$

where ω_0 is the carrier frequency. When the incident angle is close to the Littrow angle, $\theta(\omega_0) \approx 0$. Equation (2) can then be simplified to

$$\delta\varphi_{\mathrm{GD}} = 4\pi \frac{\Delta G}{d} \tan(\gamma). \tag{3}$$

Considering a typical grating with $d^{-1} = 1200$ lines/mm, a grating separation change by a half of the grating constant can result in a CEP change on the order of 2π rad, because $\gamma > 45°$ for most conventional grating compressors. However, in the configuration of the transmission grating compressor in our laser system, a smaller perpendicular distance between the gratings is used because of the smaller pulse stretch factor, which reduces the sensitivity of the CEP to beam pointing and air currents in the compressor. Moreover, according to (3), the two-fold larger grating constant and smaller incident angle (13.9°) can decrease CEP fluctuations introduced by changes in grating separation by up to 90%. Figure 4a compares the CEP drift of the compressed pulses on a short time scale with (∼194 mrad rms) and without (∼301 mrad rms) the slow feedback loop (the start of active stabilization is marked by an arrow in the figure). The compressed pulse energy is 2.2 mJ for a 750-μJ seed into the second amplifier for this acquisition. From the open-loop phase drift, it can be seen that the fast-changing noise is a bit larger than in the first amplifier (Fig. 3b), but the second amplifier and the compressor do not add significant slow drifts to the CEP. With the slow-loop feedback on, the whole laser system shows excellent and robust phase stabilization, with

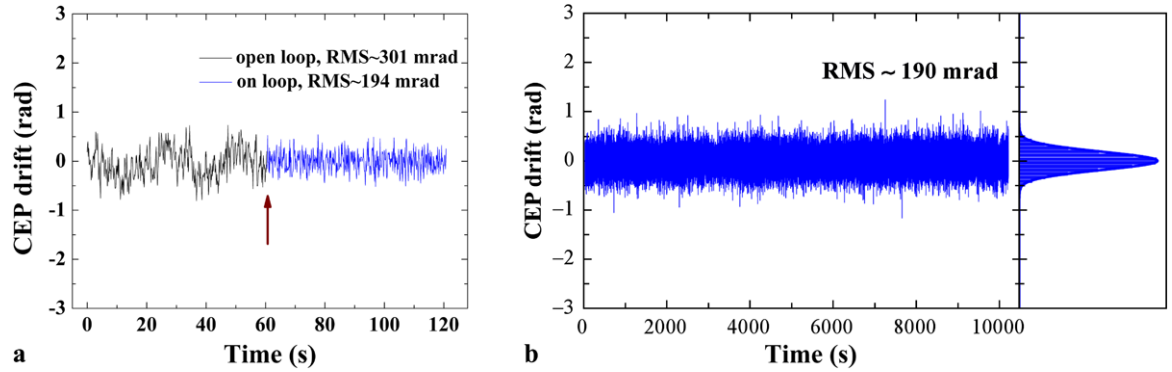

Fig. 4 CEP drift measurement of the whole laser system with 2.2-mJ, 26-fs laser output. (**a**) Comparison of CEP drift with (∼194 mrad rms, *blue line*) and without (∼301 mrad rms, *black line*) slow-loop control on a short time scale (∼1 min), with the onset of active stabilization marked by an arrow; (**b**) measured stabilized CEP drift with slow-loop control over ∼3 h (∼190 mrad rms), together with the statistical distribution of the data points over CEP drift values

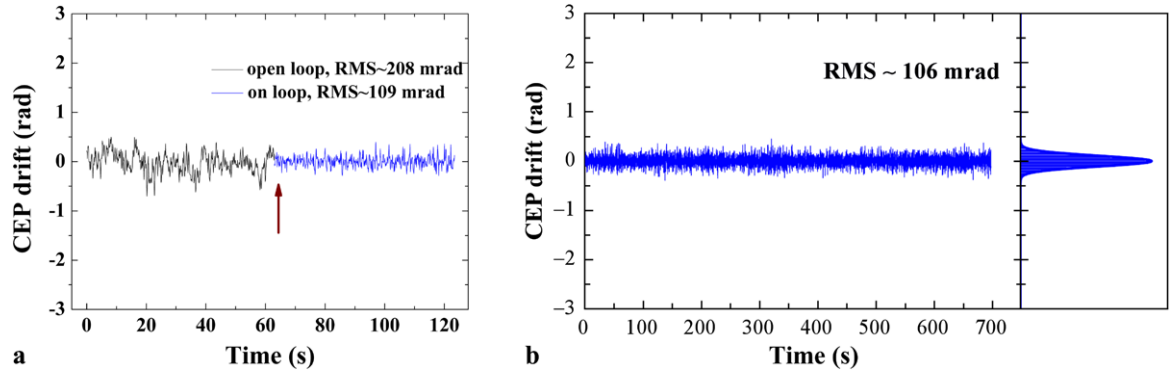

Fig. 5 CEP drift measurement of the CPA laser system for 1.65-mJ output. (**a**) Comparison of CEP drift with (∼109 mrad rms, *blue line*) and without (∼208 mrad rms, *black line*) slow-loop control on a short time scale (∼1 min), with the onset of active stabilization marked by an arrow; (**b**) measured stabilized CEP drift with slow-loop control over 12 min (∼106 mrad rms), together with the statistical distribution of the data points over CEP drift values

a rms error of ∼190 mrad measured over several hours, as shown in Fig. 4b.

The larger phase noise observed after the second amplifier can also be attributed to nonlinear phase changes coupled to intensity fluctuations in the amplifier. The introduced phase shift can vary randomly from shot to shot and cannot be pre-compensated by the slow-loop feedback. The CEP shift due to the nonlinear refractive index can be expressed as

$$\delta\varphi_{\mathrm{NL}} = 2\pi L/L_{2\pi,\mathrm{NL}}, \tag{4}$$

where L is the length of the nonlinear medium and $L_{2\pi,\mathrm{NL}}$ is the medium length corresponding to a 2π CEP shift. Considering that the refractive index is expressed as $n = n_0 + n_2 I$, for a particular intensity, I, $L_{2\pi,\mathrm{NL}}$ can be given by $L_{2\pi,\mathrm{NL}} = 1/(\mathrm{d}\Delta n/\mathrm{d}\lambda) = 1/((\mathrm{d}n_2/\mathrm{d}\lambda)I)$. Then (4) can be changed to

$$\delta\varphi_{\mathrm{NL}} = 2\pi \cdot IL \cdot \frac{\mathrm{d}n_2}{\mathrm{d}\lambda}. \tag{5}$$

We know that the B-integral is the total phase change due to the nonlinear refractive index given by $B = 2\pi/(\lambda n_0) \cdot \int_0^L n_2 I \,\mathrm{d}z$. It can be simplified to $B = 2\pi n_2/\lambda n_0 \cdot IL$, when I is assumed constant over L. Then we get $IL = \lambda n_0 B/(2\pi n_2)$, and (5) is expressed by

$$\delta\varphi_{\mathrm{NL}} = \frac{\lambda n_0}{n_2} \cdot \frac{\mathrm{d}n_2}{\mathrm{d}\lambda} \cdot B. \tag{6}$$

Then the CEP change due to the intensity fluctuation ΔI is given by $\delta\varphi_{\mathrm{NL}}\Delta I$.

The total B-integral of our laser system is about 3 for a 2.2-mJ output. In order to investigate the effect of the B-integral on the CEP in our laser system, we tested the CEP drift of the laser system for lower B-integral (∼1 rad) by seeding the second amplifier with 400 μJ and limiting the output energy to 1.65 mJ. In this case, the open-loop CEP drift of the laser system (Fig. 5a) shows smaller drift amplitude than in the case of higher output energy (Fig. 4a). The standard drift error with the slow loop on

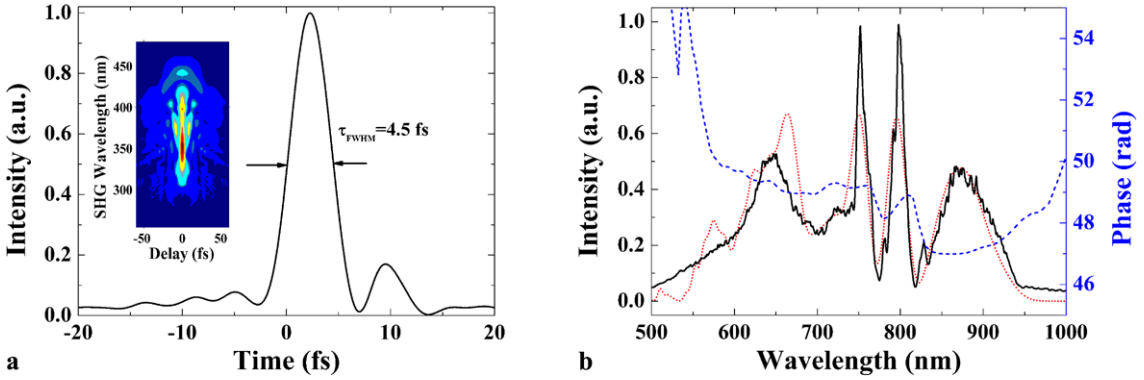

Fig. 6 Characteristics of the optimal compressed pulses after the HCF compressor with 2-1 mJ, 26-fs seed pulses and a neon pressure of 1.5 bar. (**a**) Retrieved temporal profile (4.5 ± 0.1 fs), measured by a FROG instrument; the inset is the retrieved FROG trace with a FROG error of ∼1%; (**b**) FROG retrieved spectrum (*dotted red line*) and spectral phase (*dashed blue line*), compared with the measured spectrum (*solid black line*) by a fiber spectrometer

(Fig. 5b) is dramatically reduced to 106 mrad rms over a 12-min measurement, comparable to that of the first amplifier with the commercial prism compressor. This clearly indicates that the CEP drift due to the second amplifier results mainly from nonlinear effects inside the gain crystal. Reducing the B-integral of the laser system by slightly increasing the seed stretch (to 10 ps) could help improve the long-term CEP stability even further. In the current configuration, the stretch factor is limited by the large amount of negative third-order spectral phase introduced by the compressor, which increases rapidly with the amount of second-order phase needed to compress the pulses. The compensation of all the excess third-order phase in the system is done using the AOPDF. However, the diffraction efficiency of the AOPDF decreases when high third-order phase is introduced and amplification becomes inefficient for large values of third-order dispersion (TOD) ($> \pm 150{,}000$ fs^3), setting an upper limit to the affordable stretch factor.

In fact, the B-integral of the amplifier just reflects the influence of intensity fluctuations on the CEP measurement itself. The pulse intensity instability takes its source from the front-end laser, which is strongly dependent on the stability of the pump laser. According to previous investigations, 1% pulse energy fluctuations can change the measured CEP by more than 100 mrad [14, 42], which is consistent with our single-shot measurements. However, it is worth mentioning that large CEP error points have only a minor influence of the measured long-term CEP drift.

8 Pulse compression below 5-fs duration in a gas-filled HCF

The CEP-stable, 2.1-mJ, 26-fs pulses from the amplifier were used to drive post compression in the HCF (Fig. 1). The input beam polarization can be changed between linear (LP) and circular (CP) using a broadband achromatic quarter-wave plate (QWP1). The laser beam is then carefully coupled into the HCF by an $f = +2$ m focusing mirror. The HCF is 1-m long with an inner diameter of 250 μm and rests inside a tube filled with a static pressure of neon. The output beam from the HCF can be changed from CP back to LP downstream using a second broadband achromatic quarter-wave plate (QWP2). The dispersion of QWP1 and the entrance window (300-μm-thick fused silica) of the HCF tube can be easily pre-compensated using the AOPDF. Meanwhile, the total pulse dispersion of the HCF setup including QWP2 as well as ∼2.5-m air is first slightly overcompensated by using a set of broadband chirped mirrors (Femtolasers GmbH) and then is fine tuned with a pair of fused silica wedges, set at Brewster angle, to get the shortest compressed pulses. Pulse compression is optimized and measured using a home-made, dispersion-less frequency-resolved optical gating (FROG) device that is a duplicate of that described in Ref. [43], suitable for ultra-broadband pulse characterization.

At an optimal gas pressure of 1.5 bar, 4.5-fs (±0.1-fs) pulses with 1-mJ energy are routinely generated. The typical measured temporal profile and spectrum together with the spectral phase and spectrum retrieved by the FROG are shown in Fig. 6. The estimated FROG error in the temporal pulse duration is ∼1%. The satellite pulses in the reconstructed temporal profile result from the combined effects of residual high-order spectral phase and strong modulations in the broadened spectrum. The retrieved FROG spectrum shows very good agreement with the measured spectrum as shown in Fig. 6b. The broadened spectrum supports ∼3-fs Fourier-transform-limited pulses. Spectral clipping due to the bandwidth limit of the chirped mirrors was observed in the experiment, implying that even shorter compressed pulses could be expected with broader-bandwidth chirped mirrors.

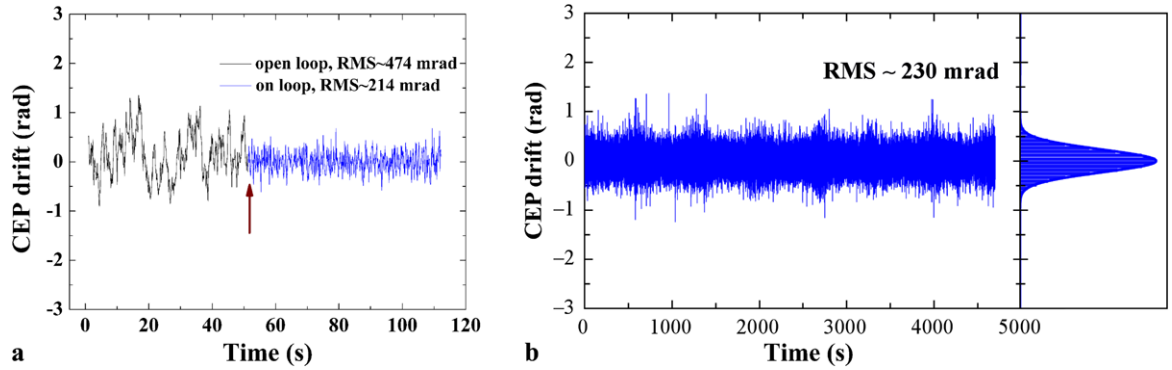

Fig. 7 CEP drift measurement of the few-cycle pulses after HCF compressor (1-mJ, sub-5-fs). (**a**) Comparison of CEP drift with (∼214 mrad rms, *blue line*) and without (∼474 mrad rms, *black line*) slow-loop control on a short time scale (∼1 min), with the onset of active stabilization marked by an arrow; (**b**) measured stabilized CEP drift with slow-loop control over 1 h (∼230 mrad rms), together with the statistical distribution of the data points over CEP drift values

The bandwidth of the sub-5-fs pulses is broad enough to allow direct CEP drift measurement without the need for any extra spectral broadening. A small part of the compressed pulses is split off and focused into a 0.5-mm-thick BBO crystal to double the IR frequency component of the spectrum, which is used to interfere with the blue part of the fundamental spectrum using a crossed polarizer. The interference fringes are acquired using a Thorlabs SPx spectrometer and the signal fed back to the APS software to calculate and stabilize the CEP drift. A short time scale open-loop measurement is shown in Fig. 7a. The CEP is quite well preserved even after a long pulse propagation distance (a few meters), but shows bigger slow drift amplitude compared to the open-loop measurement of the laser system (Fig. 4a). This mainly comes from intensity variations due to the beam pointing and energy fluctuations of the input beam. Feeding the CEP drift after the HCF back to the Menlo system electronics, the CEP of the whole laser system including the HCF compressor can be well stabilized. A typical long-term CEP drift measurement is shown in Fig. 7b, indicating a rms error of ∼230 mrad over 1 h.

Thanks to the mode confinement of the HCF, the generated sub-5-fs laser beam exhibits near-perfect spatial quality. In order to estimate the maximum intensity achievable with our system, the beam was attenuated with reflective metallic filters (factor of 100) and focused down to a 6-µm-diameter spot size (at $1/e^2$ peak intensity) using a 40-mm-diameter beam (at $1/e^2$ peak intensity) incident on an $f/4$, 30-degree, off-axis parabola. Figure 8 shows the intensity profile measured at focus using a microscope objective (magnification factor of 20). From this profile, we safely estimate that 73.7% of the incident pulse energy on the parabola is located in the central part of the focused beam (above $1/e^2$ peak intensity), indicating a Strehl ratio better than ∼0.9. Such conditions correspond to a focused intensity of more than 10^{17} W/cm^2 without wavefront correction. Note that the measurement was taken more than 6 m away from the HCF compressor output.

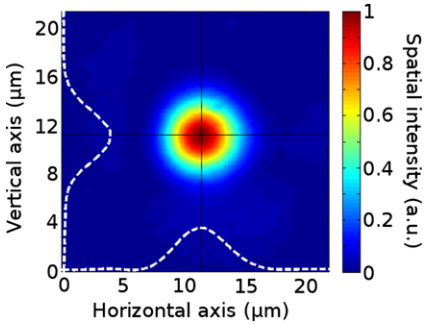

Fig. 8 Spatial intensity distribution of the full sub-5-fs laser beam under vacuum at the focus of an $f/4$ parabola

9 Conclusions and prospect

In conclusion, we presented CEP stabilization (∼190 mrad rms) of a transmission grating-based CPA system delivering 2.2-mJ, 26-fs pulses at 1 kHz and the generation of CEP stable (∼230 mrad rms), high spatial quality, sub-5-fs, mJ-level pulses by post compression in a HCF seeded with a circularly polarized laser beam. We demonstrated that reducing the optical pathway in the stretcher and compressor leads to robust long-term CEP stability of the system. A high efficiency ruled transmission-grating compressor (∼80% throughput) has been commissioned to achieve >4 mJ compressed sub-30-fs pulses. Furthermore, our post-compression technique could be scaled to multi-mJ output energies (together with CEP control) by using a bigger-core HCF filled with a pressure gradient or higher ionization threshold gases. The high pulse energy, ultra-short pulse duration, high spatial quality features of the system, combined

with the long-term CEP stability, make it a useful experimental tool for performing high-field science.

References

1. F. Krausz, M. Ivanov, Rev. Mod. Phys. **81**, 163 (2009)
2. P. Agostini, L.F. DiMauro, Rep. Prog. Phys. **67**, 813 (2004)
3. R. Kienberger, E. Goulielmakis, M. Uiberacker, A. Baltuska, V. Yakovlev, F. Bammer, A. Scrinzi, Th. Westerwalbesloh, U. Kleineberg, U. Heinzmann, M. Drescher, F. Krausz, Nature **427**, 817 (2004)
4. G. Sansone, E. Benedetti, F. Calegari, C. Vozzi, L. Avaldi, R. Flammini, L. Poletto, P. Villoresi, C. Altucci, R. Velotta, S. Stagira, S. De Silvestri, M. Nisoli, Science **314**, 443 (2006)
5. E. Goulielmakis, M. Schultze, M. Hofstetter, V.S. Yakovlev, J. Gagnon, M. Uiberacker, A.L. Aquila, E.M. Gullikson, D.T. Attwood, R. Kienberger, U. Kleineberg, Science **320**, 1614 (2008)
6. J. Nees, N. Naumova, E. Power, V. Yanovsky, I. Sokolov, A. Maksimchuk, A.W. Bahk, V. Chvykov, G. Kalintchenko, B. Hou, G. Mourou, J. Mod. Opt. **52**, 305 (2005)
7. D.F. Hotz, Appl. Opt. **4**, 527 (1965)
8. C. Le Blanc, P. Curley, F. Salin, Opt. Commun. **131**, 391 (1996)
9. M. Nisoli, S. De Silvestri, O. Svelto, Appl. Phys. Lett. **68**, 2793 (1996)
10. C.P. Hauri, W. Kornelis, F.W. Helbing, A. Heinrich, A. Couairon, A. Mysyrowicz, J. Biegert, U. Keller, Appl. Phys. B **78**, 673 (2004)
11. S. Akturk, C.L. Arnold, B. Zhou, A. Mysyrowicz, Opt. Lett. **34**, 1462 (2009)
12. F.W. Helbing, G. Steinmeyer, J. Stenger, H.R. Teller, U. Keller, Appl. Phys. B **74**, S35 (2002)
13. T. Fuji, J. Rauschenberger, A. Apolonski, V.S. Yakovlev, G. Tempea, T. Udem, C. Gohle, T.W. Hansch, W. Lehnert, A. Scherer, F. Krausz, Opt. Lett. **30**, 332 (2005)
14. A. Baltûska, M. Uiberacker, E. Goulielmakis, R. Kienberger, V.S. Yakovlev, T. Udem, T.W. Hänsch, F. Krausz, IEEE J. Quantum Electron. **9**, 972 (2003)
15. M. Kakehata, Y. Fujihira, H. Takada, Y. Kobayashi, K. Torizuka, T. Homma, H. Takahashi, Appl. Phys. B **74**, S43 (2002)
16. E. Gagnon, I. Thomann, A. Paul, A.L. Lytle, S. Backus, M.M. Murnane, H.C. Kapteyn, A.S. Sandhu, Opt. Lett. **31**, 1866 (2006)
17. Z. Chang, Appl. Opt. **45**, 8350 (2006)
18. C. Li, E. Moon, Z. Chang, Opt. Lett. **31**, 3113 (2006)
19. C. Li, H. Mashiko, H. Wang, E. Moon, S. Gilbertson, Z. Chang, Appl. Phys. Lett. **92**, 191114 (2008)
20. J.-H. Lee, Y.S. Lee, J. Park, J.J. Park, D.S. Kim, T.J. Yu, C.H. Nam, Appl. Phys. B **96**, 287 (2009)
21. L. Canova, X. Chen, A. Trisorio, A. Jullien, A. Assion, G. Tempea, N. Forget, T. Oksenhendler, R. Lopez-Martens, Opt. Lett. **34**, 1333 (2009)
22. L. Canova, A. Trisorio, X. Chen, B. Mercier, O. Albert, R. Lopez-Martens, N. Forget, T. Oksenhendler, D. Kaplan, in *CLEO 2009: Closed-loop Optimization of the Temporal Duration of a 21 fs, 4 mJ CPA Laser System With High B-integral*, Baltimore, Maryland, USA, 31 May–5 June 2009, JTuD38
23. L. Gallmann, T. Pfeifer, P.M. Nagel, M.J. Abel, D.M. Neumark, S.R. Leone, Appl. Phys. B **86**, 561 (2007)
24. A.J. Verhoef, J. Seres, K. Schmid, Y. Nomura, G. Tempea, L. Veisz, F. Krausz, Appl. Phys. B **82**, 513 (2006)
25. H. Mashiko, C.M. Nakamura, C. Li, E. Moon, H. Wang, J. Tackett, Z. Chang, Appl. Phys. Lett. **90**, 161114 (2007)
26. A. Suda, M. Hatayama, K. Nagasaka, K. Midorikawa, Appl. Phys. Lett. **86**, 111116/1 (2005)
27. J.H. Sung, J.Y. Park, T. Imran, Y.S. Lee, C.H. Nam, Appl. Phys. B **82**, 5 (2006)
28. S. Bohman, A. Suda, M. Kaku, M. Nurhuda, T. Kanai, S. Yamaguchi, K. Midorikawa, Opt. Express **16**, 16684 (2008)
29. J. Park, J.-H. Lee, C.H. Nam, Opt. Lett. **34**, 2342 (2009)
30. S. Ghimire, B. Shan, C. Wang, Z. Chang, Laser Phys. **15**, 838 (2005)
31. X. Chen, A. Jullien, A. Malvache, L. Canova, A. Borot, A. Trisorio, C.G. Durfee, R. Lopez-Martens, Opt. Lett. **34**, 1588 (2009)
32. R.W. Boyd, *Nonlinear Optics*, 2nd edn. (Academic Press, New York, 2003), p. 203
33. S. Petit, A. Talebpour, A. Proulx, S.L. Chin, Opt. Commun. **175**, 323 (2000)
34. J. Liu, X.W. Chen, R.X. Li, T. Kobayashi, Laser Phys. Lett. **5**, 45 (2008)
35. A. Trisorio, C.P. Hauri, Opt. Lett. **32**, 1650 (2007)
36. A.S. Sandhu, S. Banerjee, A. Goswami, Opt. Commun. **181**, 101 (2000)
37. H. Yang, J. Zhang, Q. Zhang, Z. Hao, Y. Li, Z. Zheng, Z. Wang, Q. Dong, X. Lu, Z. Wei, Z. Sheng, Opt. Lett. **30**, 534 (2005)
38. A. Varela, A. Zair, J.S. Roman, B. Alonso, I.J. Sola, C. Prieto, L. Roso, Opt. Express **17**, 3630 (2009)
39. T. Fuji, A. Apolonski, Opt. Lett. **29**, 632 (2004)
40. V.V. Lozovoy, B. Xu, Y. Coello, M. Dantus, Opt. Express **16**, 592 (2008)
41. K. Masayuki, T. Hideyuki, K. Yohei, T. Kenji, F. Yoshihiko, H. Tetsuya, T. Hideo, Opt. Lett. **26**, 1436 (2001)
42. C. Li, E. Moon, H. Wang, H. Mashiko, C.M. Nakamura, J. Tackett, Z. Chang, Opt. Lett. **327**, 796 (2007)
43. S. Akturk, C. D'Amico, A. Mysyrowicz, J. Opt. Soc. Am. B **25**, A63 (2008)